



Multi-dimensional characterization of groundwater distribution in sub-Himalayan region of Pakistan

Ali Yousaf Khan¹ · Abrar Niaz¹ · Umair Bin Nisar²

Received: 22 August 2023 / Accepted: 4 December 2023 / Published online: 4 January 2024
© The Author(s), under exclusive licence to Springer-Verlag GmbH Germany, part of Springer Nature 2024

Abstract

The groundwater scarcity, lack of scientific approaches, and increasing number of unsuccessful boreholes coupled with climate change are crucial issues faced in sub-Himalayan region. Integrated geophysical techniques of electrical resistivity and magnetotelluric survey in conjunction with hydrochemical analysis were utilized at Rawalakot city and adjoining areas of sub-Himalayan region to demarcate groundwater potential, identify water-bearing fractured lithologies, and aquifer vulnerability along with water quality. Due to structural complexity, subsurface lithological units demarcated by electrical resistivity survey included broad spectrum of lithologies consisting of topsoil, clay, boulder, sandstone, mudstone, siltstone, gravel, and sandy gravel that resemble closely to the available borehole data. Different aquifer zones were identified in the southern portion of the study area with most aquifers as unconfined in nature. The overall apparent resistivity fluctuates between 0.001 and 7118 Ω -meters with 40 to 60 Ω -meters in aquifer zone. The aquifer thickness ranges from 20 to 180 m in the subsurface, while 2D-AMT models also reveal the maximum depth of fractures up to 200 m. The 2D sections of electrical resistivity were compared with 2D magnetotelluric profiles to enhance the identification of subsurface lithology, structural elements as well as the aquifer potential in the study area. The pseudo-sections acquired from the electrical resistivity survey and magnetotelluric profiles were in accordance with each other. To validate the geophysical results with groundwater quality, 39 water samples were acquired from different localities in the study area, among which 16 samples were marked as unsafe for drinking, whereas 23 samples were marked as safe.

Keywords Aquifer characterization · Audio-magnetotelluric · Contamination · Electrical resistivity · Groundwater modeling · Rawalakot

Introduction

Water is only inorganic liquid that exists in three states, e.g., solid, liquid, and gas. It plays a significant role in occurrence of all aspects of life (Franks 2000; Makhmudov et al. 2021). Increase in population and climate change is severely

affecting the water quality and quantity on planet earth. The situation gets worse in developing country like Pakistan which is among top ten countries severely affected by climate change (Hujakulova et al. 2021). The sub-Himalayan region due to its hard terrain and increasing population faces several challenges among which availability of potable water for domestic and industrial use is primary. Industrial growth is also introducing harmful chemicals in the local aquifer system that is deteriorating the quality of water (Nisar et al. 2021). Addressing these problems requires holistic approaches that combine science with social aspects.

Geophysical techniques have been used for centuries to demarcate water-bearing zones (Nisar et al. 2023). There are multiple surface-based geophysical techniques, which are used to explore subsurface water. These techniques include electrical resistivity, surface nuclear magnetic resonance, and telluric surveys (Singh and Sharma 2023). Geospatial techniques are also widely used for groundwater resource

✉ Abrar Niaz
abrar.niaz@ajku.edu.pk

Ali Yousaf Khan
ali.yousaf.geo@ajku.edu.pk

Umair Bin Nisar
Umair.nisar@comsats.edu.pk

¹ Institute of Geology, The University of Azad Jammu and Kashmir, Muzaffarabad, Pakistan

² Department of Meteorology, COMSATS University Islamabad, Park Road, Tarlai Kalan, Islamabad 45550, Pakistan

exploration and development (Gautam et al. 2023). The integrated geophysical techniques like vertical electrical sounding, time-domain electro-magnetic methods along with micro-gravity surveys are useful for the assessment of groundwater resources (Mohamed et al. 2023). These integrated studies involve several geological factors, such as fractures, faults, and lithologies that control the local groundwater distribution (Agyemang 2022; Nair et al. 2022). The vertical electrical sounding in conjunction with controlled source audio-frequency magnetotelluric (CSAMT) is most used in various exploration problems, such as subsurface structural and fault mapping as well as groundwater exploration around larger depths. This integration is mostly accurate and often requires much less budget and labor. In comparison, other geophysical methods have ambiguities and uncertainties unless exact fracture point is not given to them. The integration of these techniques can reduce the rate of unsuccessful drilling (Agyemang 2020; Chouteau et al. 1994; Kouadio et al. 2022; Li et al. 2017).

With increase in industrial activities the groundwater quality is also facing serious threat (Suleman et al. 2023). Most of the industrial zones introduce harmful chemicals into nearby streams or open spaces that eventually find their path to subsurface shallow aquifer system (Nisar et al. 2023). These contaminants range from microbial to heavy metals (Nisar et al. 2021). To understand the distribution of contamination in the subsurface, integrated approach of geophysical and hydrochemical methods is applied to identify the extent of subsurface contamination (Hasan et al. 2023).

The study area lies at the municipality of Rawalakot city and its adjoining areas, which is the part of District Poonch, Azad Kashmir (Fig. 1). Tectonically, the study area lies in Sub-Himalaya. The study area is about 20 square kilometers and located between latitude 33.855814°, 33.850082°; and longitude 73.70°, 73.737740°. With growing population, hard terrain, and soaring temperatures, the community of the area faces serious threat related to potable water availability for domestic as well as industrial purposes. The

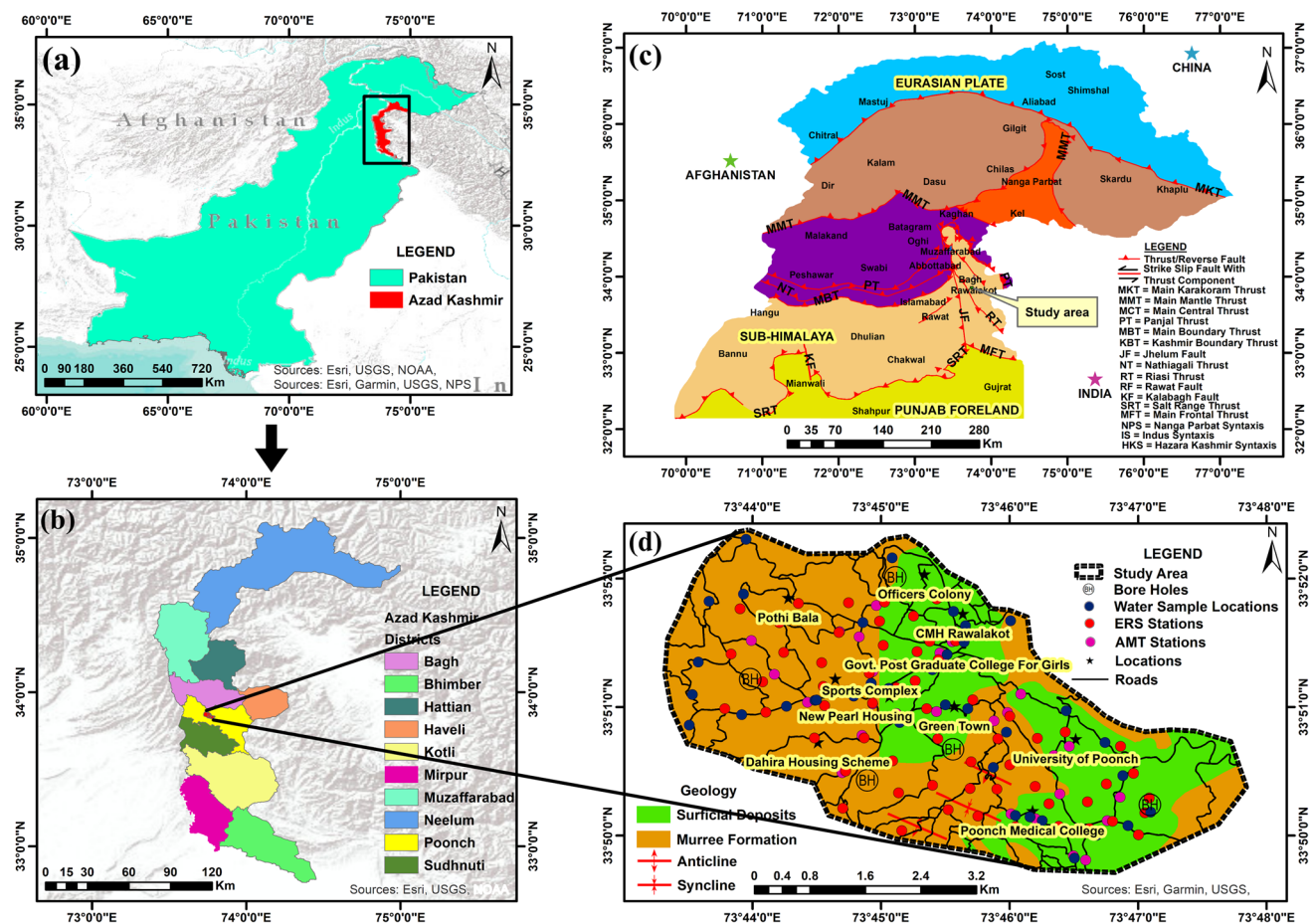


Fig. 1 a Location map of Azad Kashmir in Pakistan shown by red polygon. b Figure showing Azad Kashmir with Poonch District represented by yellow color polygon. c The tectonic map of northern Pakistan with study area compiled after (Calkins et al. 1975; Chaudhry

et al. 1997; Hameed et al. 2023; Khan et al. 2016; Searle et al. 1996; Wadia 1931). d The geological map of the study area (compiled and modified after Hussain et al. 2014, 2004)

tough mountain terrain makes the water availability difficult, and the industrial development is making already available resources contaminated. The present study focuses in addressing these problems with the integration of electrical resistivity and audio-magnetotelluric methods for the demarcation of subsurface lithology, their lateral and vertical extension, depth, and thickness of different water-bearing layers, shallow and deep-seated rock features. Previous researchers in the area utilized an electrical resistivity method, which keeping in view the hilly terrain has several ambiguities and often required close integration with other data sets which at most of time was not available. This integration will help in identifying the new and accurate groundwater bearing zones. The geo-chemical analysis will be carried out to investigate the quality of groundwater. The contamination from industrial as well as domestic sources has been catered and classified in close coordination with the geophysical surveys. The research will be of particular interest to the scientific readers, Government decision-making authorities, and local community.

Study area

Geological and tectonic setting of the study area

The current study is part of District Poonch, Azad Kashmir. Tectonically, the study area is part of Sub-Himalaya, Pakistan (Fig. 1c). Multiple active fault lines pass through the vicinity of the study area. The northern Pakistan has number of disastrous earthquakes especially the 8th October, 2005 earthquake which initiated with Magnitude 7.5 and jolted the Muzaffarabad, Bagh, and Rawalakot areas of Azad Kashmir (Lisa et al. 2006). The Riasi thrust passes near the study area. The recent mapping demarcated the presence of active emergent thrust faulting occurring within the fold-and-thrust belt north of the deformation thrust front in the NW Himalaya. The > 60-km-long Riasi fault system is the southeastern most segment of a seismically active regional fault system that extends more than 200 km stepwise to the southeast from the Balakot-Bagh fault in Pakistan into northwestern India (Gavillot et al. 2016).

The study area consists of a narrow valley surrounded by hills and mountains with elevation ranging from 1544 to 1790 m from the sea level. The main source of the groundwater recharge is the meteoric water with maximum of 476 mm in the summer season. Two geological formations lie in the study area which is Murree Formation (Rawalpindi Group) of Early Miocene age and surficial deposits of Recent age. The Murree Formation is mainly composed of red to purple and greenish grey sandstone, siltstone, purple to reddish brown mudstone and conglomerate, while the surficial deposits are composed of unconsolidated deposits

of sand, silt, clay, and gravels (Latif 1970; Shah 2009). The conglomerates of Murree Formation and gravels of surficial deposits act as aquifer in the study area.

Methodology

The present work involves extensive resistivity, audio-magnetotelluric and hydrochemical data acquisition. ABEM SAS Terrameter 4000 was used for the acquisition of the 1D electrical resistivity survey, while the PQWT TC-500 was used for the acquisition of the 2D audio-magnetotelluric data in the study area. A total number of 67 Vertical Electrical Soundings, 34 AMT Profiles, and 40 water samples were acquired from the field to investigate the groundwater potential and water quality of study area. Different computer softwares were used for the processing of ERS and AMT data. Arc GIS (10.4.1) was used for the compilation of geological maps, Rockworks (16) was used for the generation of 3D models of study area, and the Surfer (16) Golden Software was used for making different isopach apparent resistivity and magnetotelluric data as well as the 2D profile. Similarly, Strater (5) Golden Software was used for making the interpreted lithologies, IPI2WIN software (Bobachev 2003) was used for the processing of 1D ERS data, and Google Earth Pro was used for plotting the field data in the laboratory.

The whole work was divided into three phases. Phase 1 was to conduct the 1D Vertical Electrical Sounding (VES) in the study area within the space that was available. A large part of the city was covered with construction; however, the VES stations were established at available space intervals. The ERS data were processed to generate apparent resistivity curves, apparent resistivity maps at different depths, 3D lithological models, 3D inversion model, and pseudo-resistivity sections. The apparent resistivity maps at MN and AB (current and potential electrodes) electrode spacings were prepared using the Golden Software (Surfer 16) using the minimum curvature and convex hull as the study area was in hilly terrain and maximum space was covered. The second phase was comprised of Audio-Magnetotelluric survey data compilation. The time was selected for the acquisition of 2D-AMT data as time factor majorly influence the quality of the AMT data (Hermance et al. 1975; Kelbert et al. 2017; Kirkby 2019; Rosas-Carbajal et al. 2015; Simpson et al. 2021). The 2D profile data were then processed to convert 1D data to co-relate with 1D VES results. Several isopach maps of AMT data and 3D inversion model of AMT data were also generated. The third phase was comprised of collection of water samples from the municipality of Rawalakot city according to the International standards (Gelsey et al. 2023; Hayder et al. 2023; Hespanhol et al. 1994; Javaid et al. 2023; Lee et al. 1982; Nyambar et al. 2023; Rahman et al. 2023). Thirty-nine water samples were collected from the study area and its adjoining areas. The chemical analysis

including color, electrical conductivity, pH, turbidity, bicarbonate, calcium, hardness, chloride, magnesium, sulphate, nitrate, sodium, potassium, alkalinity, and total coliforms were performed to ensure the quality of groundwater.

Results and discussion

Borehole lithologs

The borehole lithologs were acquired from five locations in the study area represented by BH-01–05 (Fig. 1d). The borehole BH-01 was at the northern portion of the study area and situated in the vicinity of Officers Colony. The borehole BH-02 was at the western portion of the study area near the Khrick Road, the borehole BH-03 and BH-04 were at the middle portion of study area near Ghazi-Millat Road and Green Town areas, respectively. Above-mentioned all four boreholes were on Murree Formation and contain topsoil, boulder clay, sandstone, sandstone (weathered), dry sandy soil, sandy clay, and mudstone. The borehole BH-05 was at

the southeastern portion of the study area near the University of Poonch, Rawalakot. This borehole was at the surficial deposits and comprised of unconsolidated deposits of clay, silt, sand, and gravel, respectively. All borehole lithologs with their depth and lithology are shown in Fig. 2. The weathered sandstone of BH-01, BH-02, BH-03, and BH-04 acts as an aquifer (water-bearing potential rock), while the sand and gravels (saturated) are acting as an aquifer (water-bearing rock unit).

1D electrical resistivity survey

The analysis of 1D vertical electrical sounding revealed the presence of three-to-five subsurface lithological layers. The coordinates along with true resistivity, thickness, depth, and different geoelectrical parameters are given in Table 1. The different subsurface lithological layers include topsoil, clay, clay (very dry), boulder clay, clayey sand, sandy clay, dry sandy soil, siltstone, mudstone, sandstone, sandstone (weathered), gravel (saturated), and sand and gravel (saturated). The apparent resistivity values from 0 to 10 Ω m

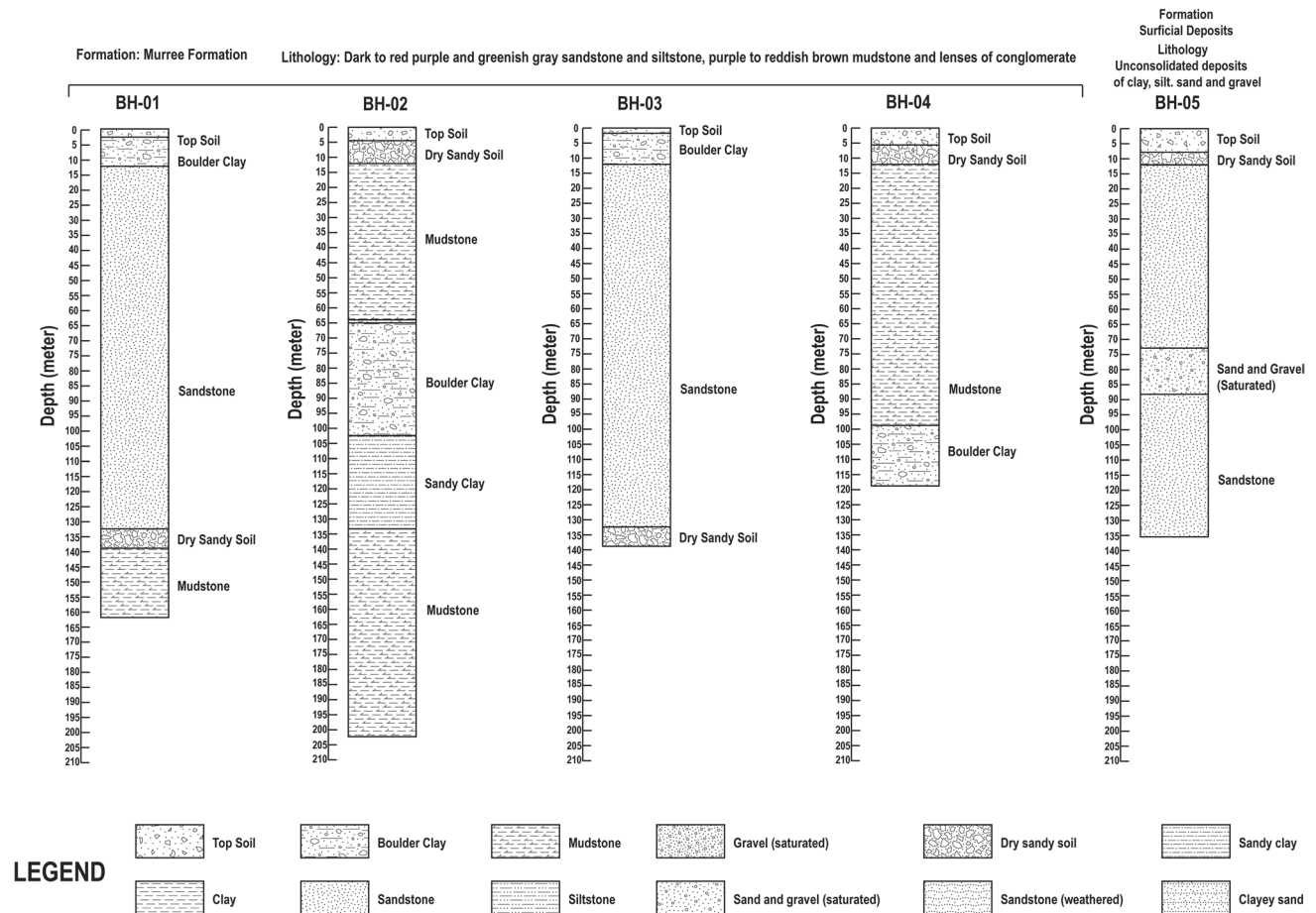


Fig. 2 Lithologs of boreholes obtained from the study area

Table 1 Modified longitudinal conductance/protective capacity rating (Nisar et al. 2018)

Longitudinal Conductance (mhos)	Protective Capacity Rating
> 10	Excellent
5–10	Very good
0.7–4.9	Good
0.2–0.69	Moderate
0.1–0.19	Weak
< 0.1	Poor

are interpreted as clays, while the lithological layers with 15–35 Ωm resistivity values are interpreted as layers of boulder clays. The layers with resistivity values ranging from 20 to 150 Ωm are interpreted as siltstone and mudstone, respectively. The apparent resistivity values ranging from 50 to 200 Ωm are interpreted as weathered sandstone, whereas the subsurface lithological bodies with resistivity values from 200 to 5000 are interpreted as layers of sandstone. The aquifer thickness values obtained by VES range from 5.28 to 184.38 m at VES 53 and VES 9, respectively. The high and low resistivity values are interpreted in terms of low and high groundwater potential in the study area (Niaz et al. 2021, 2016, 2018, 2017).

Qualitative Interpretation

Apparent resistivity maps

The presence of groundwater can be efficiently predicted by the apparent resistivity values in the subsurface. The various iso-apparent resistivity contour maps can represent the groundwater potential at different depth ranges (Moulds et al. 2023). Different isopach apparent resistivity maps including 2, 6, 10, 20, 30, 40, 50, and 80 m, respectively are shown in Fig. 3. All the apparent resistivity maps show that there are intermediate-to-hard rocks on the northwestern side of the study area. Low resistivity rocks which are associated with surficial deposits are present at the southeastern part of study area which lead to the groundwater potential zones. The subsurface layers as well as their thickness and curve types are shown in Table 1, whereas the geoelectrical and geohydrological parameters are given in Table 2.

Quantitative interpretation

Dar–Zarrouk parameters

The Dar-Zarrouk parameters were evaluated through electrical resistivity survey outcomes. This survey is very useful for demarcating subsurface lithological features; however, same lithologies may exist which may increase the ambiguities and

uncertainties in results (Hasan et al. 2019). To minimize these ambiguities, the Dar-Zarrouk parameters named as longitudinal conductance and transverse resistance have been successfully applied to the present research work. The combination of geoelectrical layers thickness and resistivity can be used in aquifer protection assessment as well as evaluation of hydrologic properties of an aquifer (Henriet 1976). The protective capacity of clayey overburden is directly related to the parameter of longitudinal conductance which is denoted as “S”.

Longitudinal conductance

The term longitudinal conductance is one of the most commonly used geoelectrical parameter which means the total conductance that took place in the direction of bedding plane of 1 m (Mohammed et al. 2023). The symbol “S” is generally used for the representation of the longitudinal conductance (Niaz et al. 2013). The longitudinal conductance is represented by the following formula:

$$S = \frac{h1}{\rho1} = \frac{h2}{\rho2} \tag{1}$$

$$S = \sum_{n=1}^n \frac{hn}{\rho n}, \tag{2}$$

where “h” and “ρ” stand for thickness and true resistivity of each layer, respectively. The longitudinal conductance is of vital importance as it is reciprocal of resistance and indicates the groundwater potential in the subsurface (Adeniji et al. 2023). The longitudinal conductance values range from 0.01 to 280 Siemens (Fig. 4a). The longitudinal conductance map of the study area is divided into five lows and six high valued areas. The H1, H2, H3, H4, H5, and H6 are areas with high longitudinal conductance values, while L1, L2, L3, L4, and L5 are areas with low longitudinal conductance values. The high values of longitudinal conductance are distributed at central and southern portion of study area showing the groundwater potential while the low values are distributed at northern portion of the study area.

Transverse resistance

The transverse resistance of any resistive layer and conductance of conducting layer are measured in the terms of transverse resistance and longitudinal conductance (Nisar et al. 2018). It is represented by the alphabetical letter “T.” It is represented mathematically as follows:

$$T = h_1\rho_1 + h_2\rho_2 + \dots \dots h_n\rho_n \tag{3}$$

$$S = \sum_{n=1}^n hn \times \rho n, \tag{4}$$

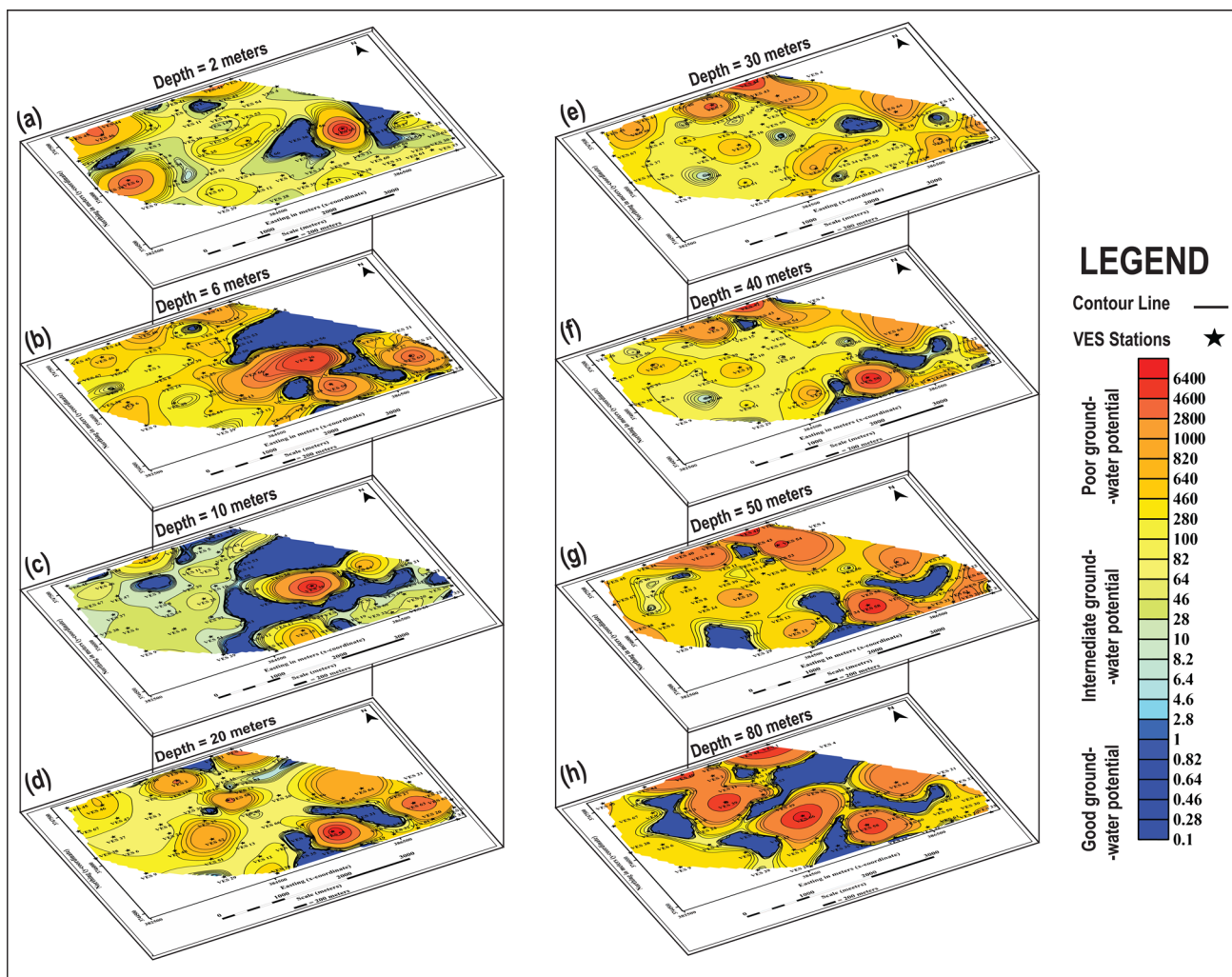


Fig. 3 Iso-apparent resistivity map at various electrodes spacing: **a** 2 m, **b** 6 m, **c** 10 m, **d** 20 m, **e** 30 m, **f** 40 m, **g** 50 m, and **h** 80 m

Table 2 Source wise distribution of water samples

Sources	No	Unsafe	Safe	%	Causes
Bore water	28	08	20	28	EC, Turbidity, pH, Calcium, Hardness
Spring water	09	08	01	88	Sulphate Nitrate, Sodium, Potassium
Filter plant	02	00	02	0	–

where “ ρ ” and “ h ” stand for true resistivity and thickness of each layer in the subsurface (Ako et al. 1986; Arulprakasam et al. 2013; Nwachukwu et al. 2019). The transverse resistance map is shown in Fig. 4d. The transverse resistance map of the study area is divided into four highs and five lows. The

areas with high values of transverse resistance, e.g., H1, H2, H3, and H4, are distributed on northwestern and southwestern portion of study area which are associated with the low groundwater potential. Whereas, the areas with low values of transverse resistance, e.g., L1, L2, L3, L4, and L5, are distributed at central and southern portion of study area which are associated with the good groundwater potential (Azeem et al. 2021; Mahmud et al. 2022; S. Singh et al. 2021).

Unit longitudinal conductance

The unit longitudinal conductance plays an important role in the overburden protective capacity ratings of the area (Obiora et al. 2015). The unit longitudinal conductance map of the area is classified into 6 lows and three highs. The H1 area is situated on the northwestern portion of study area with high value of unit longitudinal conductance, H2 and H3 areas are distributed on the central portions of study area.

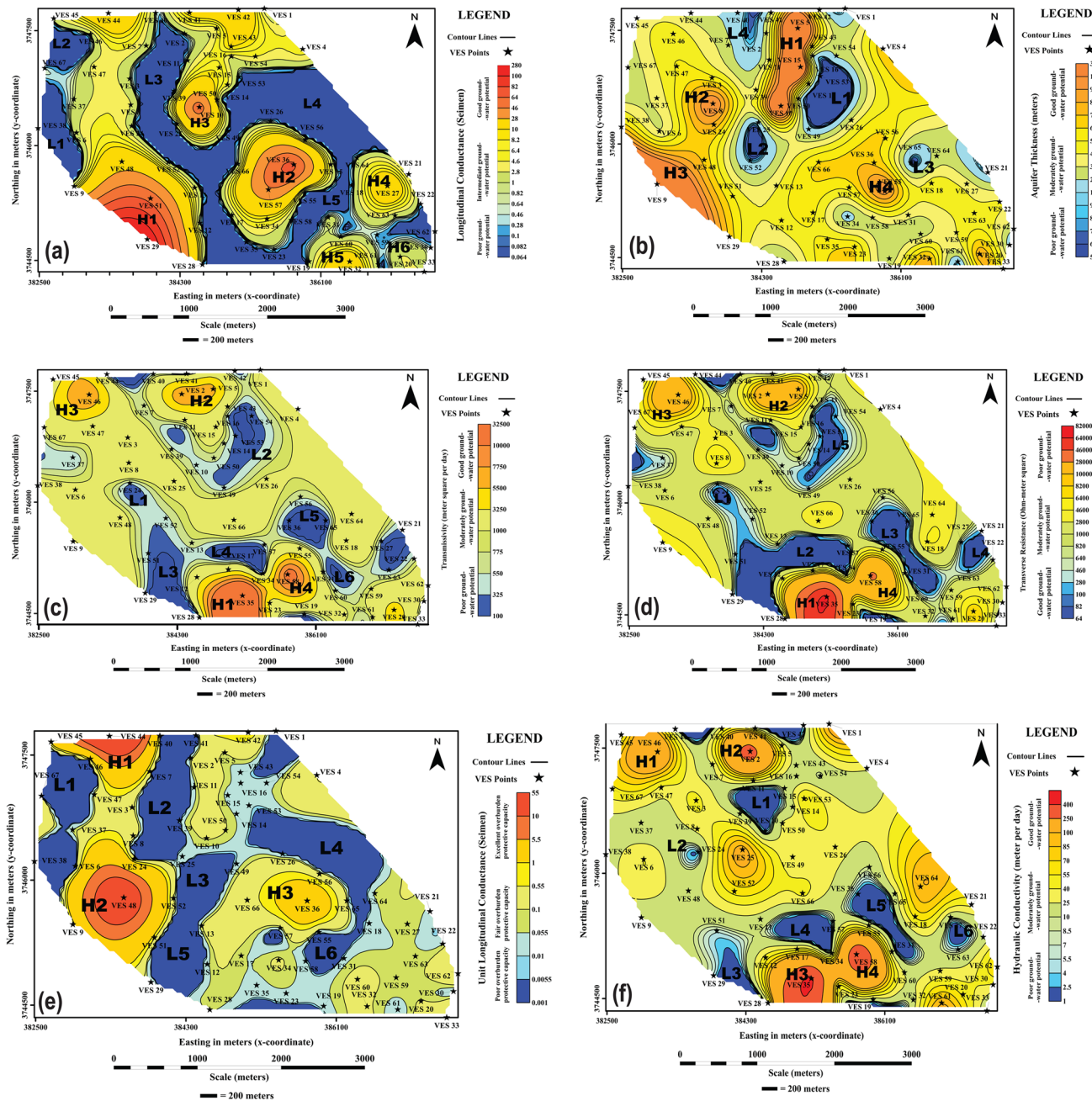


Fig. 4 Geo-electrical parameters of the study area. **a** longitudinal conductance, **b** aquifer thickness, **c** transmissivity, and **d** transverse resistance. Geo-electrical parameters of the study area. **e** Unit longitudinal conductance. **f** Hydraulic conductivity

These areas with high values of unit longitudinal conductance are categorized as good overburden protective capacity ratings which are associated with less vulnerable to leached toxic fluids from surface (Nisar et al. 2021) (Fig. 4e). Whereas the L1, L2, L3, L4, L5, and L6 areas are distributed on the central and southern portions of study area. These areas with low values of unit longitudinal conductance are categorized as the low or poor overburden protective capacity ratings which are associated with high vulnerability of

leached toxic fluids from the surface (Table 1) (Chukwuma et al. 2015).

Aquifer thickness

The aquifer thickness map of the study area is represented in Fig. 4b. The total aquifer thickness map was prepared by processing of apparent resistivity data (Nowroozi et al. 1999; Muchingami et al. 2012). The aquifer thickness map can be

visualized in terms of the groundwater volume controlled by subsurface rocks (Arshad et al. 2007; Hamzah et al. 2006; Riwayat et al. 2018). The aquifer thickness map is divided into four high and three low areas. The H1, H2, H3, and H4 areas are classified as good groundwater potential zones which are associated with good depth for accumulation of groundwater. These high groundwater potential zones have groundwater depth ranging from 70 to 180 m. Whereas, on the other side, the L1, L2, and L3 areas are classified as low groundwater potential zones which are associated with low depths for the accumulation of groundwater. These low groundwater potential zones have depth ranging from 20 to 70 m in the subsurface. Most of the aquifers were demarcated as unconfined in the study area.

Hydrogeological parameters

Total transmissivity

The total transmissivity map of the study area is shown in Fig. 4c. The total transmissivity of any area play a vital role in the hydro-geological properties of area (Ako et al. 1986); (Torrese et al. 2013); (Utom et al. 2012). The total transmissivity map of the study area is classified into four highs and low areas. The H1, H2, H3, and H4 are areas with high values of transmissivity and situated on the central and southern portion of the study area. These high values of transmissivity show the good groundwater potential due to the presence of unconsolidated surficial deposits exposed on the southern portion of study area. The L1, L2, L3, and L4 are areas with low values of transmissivity values. These areas are distributed on the central and northern portion of study area demarcating the lack of groundwater potential in these areas (Yeh et al. 2006).

Total hydraulic conductivity

The groundwater potential of any area mainly depends upon the hydraulic conductivity which is an important hydrogeological parameter (Mualem 1986). The hydraulic conductivity has strong relationship with groundwater bodies that helps us to understand the groundwater system in the subsurface (Gernez et al. 2019; Lu et al. 2021; Slater 2007; Troisi et al. 2000). The current study area is classified into four highs and six lows (Fig. 4f). The H1, H2, H3, and H4 areas are classified as high groundwater potential zones due to the high values of hydraulic conductivity, whereas the L1, L2, L3, L4, L5, and L6 are the areas with low hydraulic conductivity values that leads to the low groundwater potential in the study area. The elevated values of hydraulic conductivity are associated with unconsolidated surficial rocks deposited in the southern portion of study area, while the low values

of hydraulic conductivity are associated to rocks with low permeability.

Lithology models

The 3D lithology model was prepared on the Rockworks (16) (RockWare 2023). The interpreted model based on the resistivity data revealed the presence of 3–5 subsurface lithological layers which are boulder clay, clay, dry clay, clayey sand, dry sandy soil, gravel (saturated), mudstone, sand and gravel (saturated), sandstone, sandstone (weathered), sandy clay, siltstone, and top soil (Fig. 5a). Confined aquifers are observed on the northeastern side of the study area, whereas unconfined aquifers are demarcated mostly on southwestern side of the study area. The inversion of ERS data was executed in Arc-GIS Pro software to view the image of subsurface rocks by the means of electrical resistivity, as shown in Fig. 5b. The inversion model shows the distribution of different rock materials in subsurface up to the depth of 80 m. The interpreted lithological model and inversion model match closely to each other. The mudstone is distributed on the central and eastern parts of study area as shown by the lithology model in Fig. 5a.

Lithology projected sections

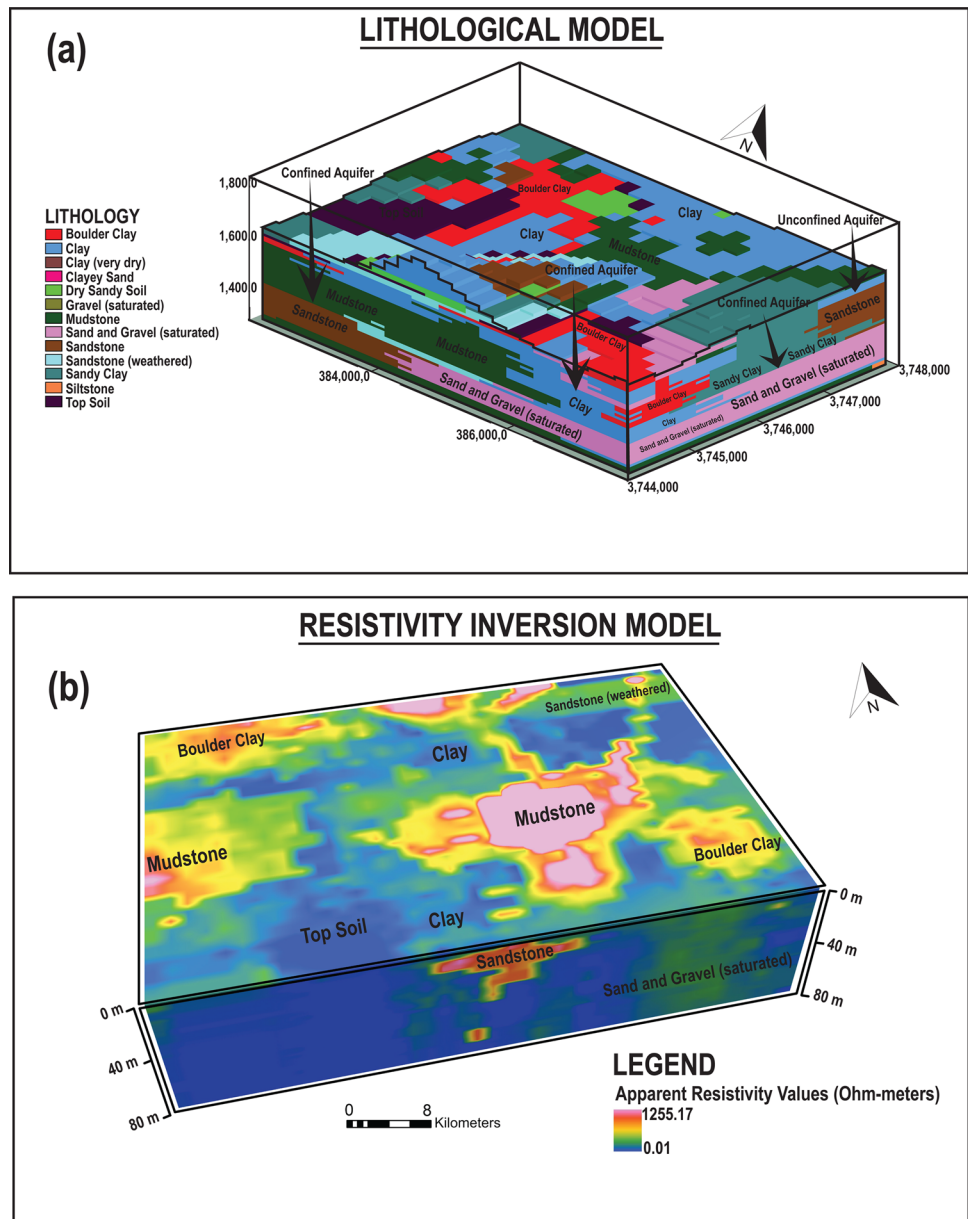
Figure 6 shows the base map of the study area showing all VES stations with both profiles A–A' and B–B'. The profile A–A' is taken in north to south direction, while B–B' profile is taken from west to east direction. The lithological units demarcated in the subsurface lithology projected sections are boulder clay, clay, clay (very dry), clayey sand, dry sandy soil, gravel (saturated), mudstone, sand and gravel (saturated), sandstone, sandstone (weathered), sandy clay, siltstone, and topsoil (Fig. 5b) (Hidayatika et al. 2022; Sajadi et al. 2013; Uwiringiyimana 2019). Both profiles also represent the subsurface lithology with best fit of all VES stations lithology with maximum sandstone, mudstone, and clay.

Audio-magnetotelluric survey

2D audio-magnetotelluric profiles

The magnetotelluric survey depicts the subsurface image of rocks and their structures by inferring the total variations in their electric and magnetic fields. This variation makes the interpreter enable to observe subsurface lithological bodies and their structures, including contacts, fractures, etc., that may lead to the accumulation of the groundwater system, especially in the hilly terrain (Aizawa et al. 2009; Huang et al. 2021; Mekkawi et al. 2022; Xu et al. 2020). A total of 34 audio-magnetotelluric profiles were taken in

Fig. 5 **a** Lithological model of the study area. **b** Apparent resistivity inversion model of the study area



the study area to validate the results of electrical resistivity survey (Fig. 7a). The seven AMT profiles (A-6, A-9, A-7, A-8, A-11, A-19, and A-1) were joined to form southwest–northeast oriented W–W’ profile, the six AMT profiles (A-3, A-15, A-12, A-8, A-26, and A-30) were joined to form north to south oriented X–X’ profile, and the seven AMT profiles (A-33, A-17, A-10, A-7, A-26, A-23 and A-24) were joined to form northwest–southeast oriented Y–Y’ profile, while the five AMT profiles (A-30, A-22, A-23, A-27, and A-28) were joined to form southwest-to-northeast oriented Z–Z’ profile. These four AMT profiles were plotted in the Move 2D software (Bremmer et al. 2016) to understand the lithology and structural elements of subsurface rocks that may lead to the groundwater accumulation (Fig. 7).

Figure 7b shows the 3D lithological diagram of subsurface rocks as well as their structures and fractures and contacts of different lithological units. Each profile is presented separately, to understand the subsurface lithological units as well as their horizontal and vertical discontinuities. Figure 7b represents the iso-anomaly contour map of southwest-to-northeast oriented Profile W–W’. The loose to intermediate strata is distributed over the profile from start to end with depth ranging from 20 to 150 m in the subsurface. The hard strata (sandstone) are distributed over the profile with depth ranging from 100 to 400 m in the subsurface. The second iso-anomaly contour map of Profile X–X’, which was north to south oriented, shows the potential difference (mV) values from 0.003 to 20. This profile contains almost hard strata up

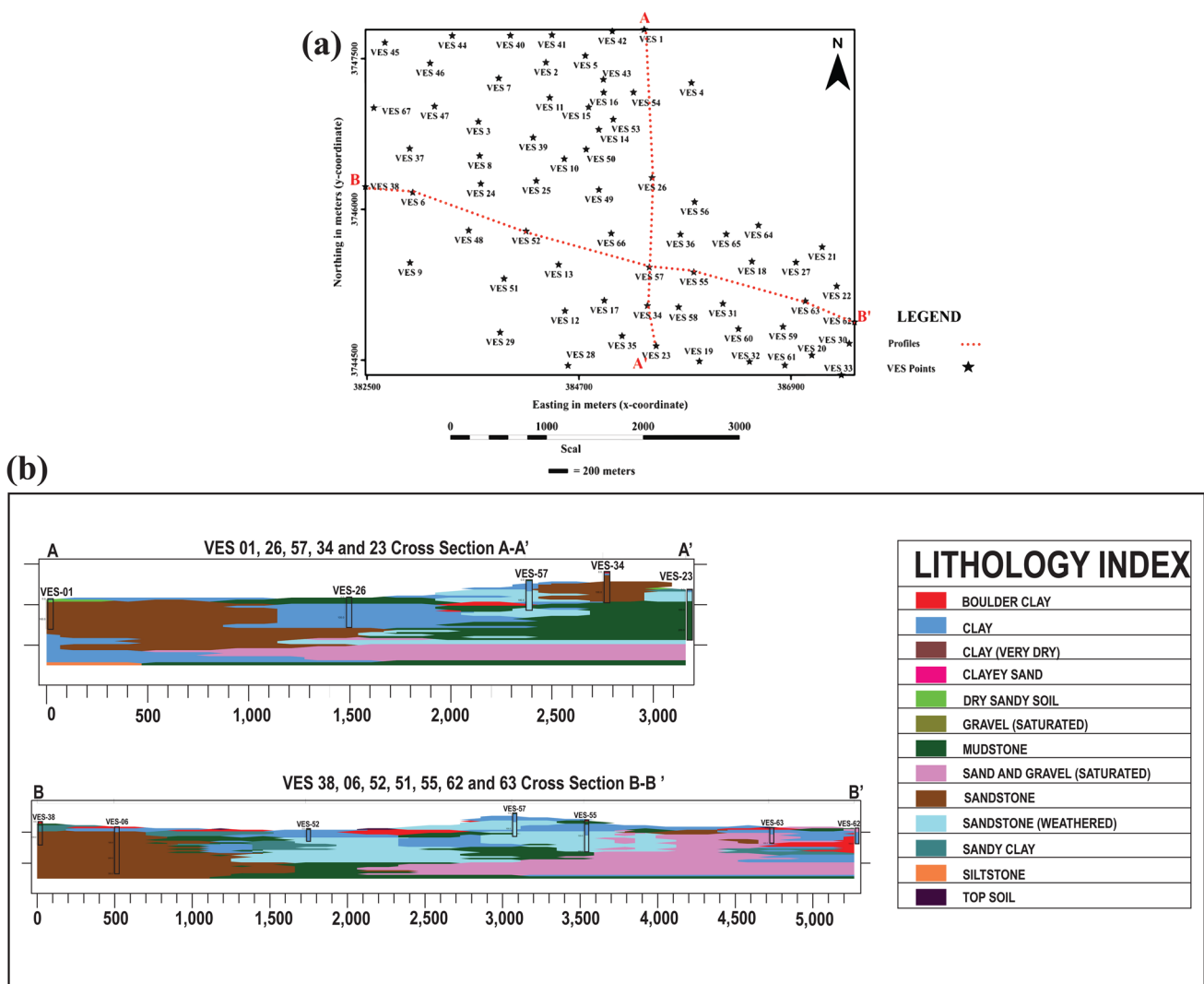


Fig. 6 a Base map of the study area showing all VES stations with both profiles A–A’ and B–B’. b Lithology projected sections A–A’ (VES 01, 26, 57, 34, and 23) and B–B’ (VES 38, 06, 52, 51, 55, 62, and 63)

to the depth of 400 m in the subsurface with no lateral or vertical discontinuities.

The third iso-anomaly contour map of Profile Y–Y’ was established in west-to-east direction (Fig. 7b). The values of potential differences range from 0.01 to 20 mV all over the profile. Different zones are marked on the profile map. The loose material/low resistivity material was demarcated from Point Number 57 to Point Number 77 on the profile map. This low resistivity material extends up to the depth of 300 m in the subsurface. There was a cavity which was identified at the depth of 250 m at Point Number 29 of the profile map. Similarly, the fourth iso-anomaly contour map of Profile Z–Z’ was conducted in southwest-to-northeast direction. The values of potential differences range from 0.003 to 50 mV with highest values towards the end portion of the profile map. The low resistivity material is distributed

from Point Number 21 to Point Number 54 up to the maximum depth of 100 m in the subsurface.

1D audio-magnetotelluric survey

The 2D audio-magnetotelluric profiles were converted into 1D data to prepare the iso-anomaly contour maps at different depths in the study area. These iso-anomaly maps at different depths enabled us to observe the subsurface lithology from shallow surface up to the depth of 500 m. Keeping in view the other active geophysical survey (1D electrical resistivity survey), their limitations, and applications, the AMT survey was immensely helpful to understand the subsurface lithology and to compare the results of lithologs and different subsurface lithological layers with each other. Figure 8 shows the contour and iso-anomaly contour maps

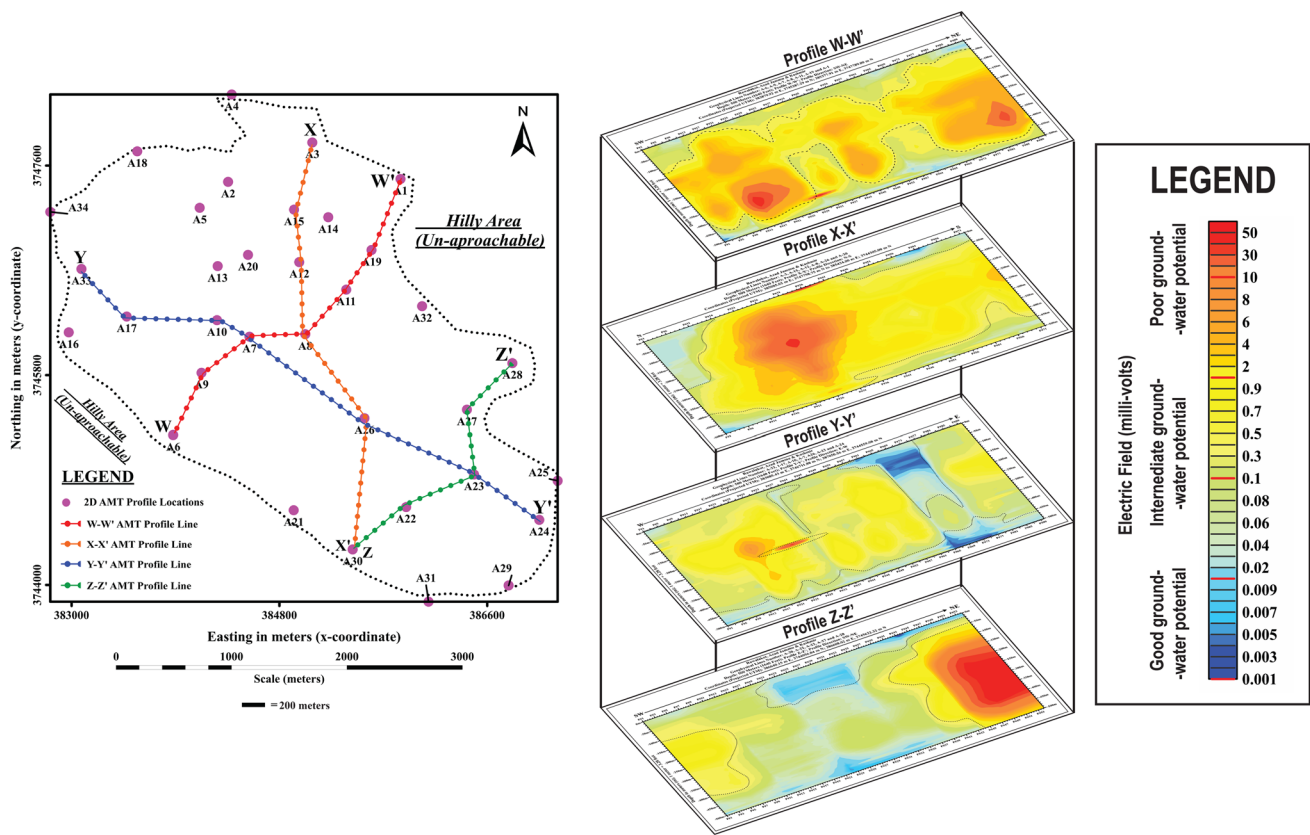


Fig. 7 a The base map of study area with W–W', X–X', Y–Y', and Z–Z' 2D audio-magnetotelluric profiles; b overlay of above-mentioned four profiles

of all AMT stations. These maps give valuable information about the change of electric field which is associated with diverse types of sedimentary rocks in the study area. All these contour maps and grid vector hill shaded relief maps show that in the shallow surface, the groundwater potential is present at the southeastern part of the study area. As the depth increases, this closure of low resistivity tends to increase up to the depth of 450 m which is associated with good groundwater potential in the study area.

Figure 8 represents the iso-anomaly contour maps of audio-magnetotelluric data from 9 m to the depth of 80 m. The iso-anomaly contour map of 8 m shows one closure of high electric field values in the extreme northern part of study area which is associated with the presence of hard/compact rocks. It also has the one closure of low electric field values at the central part of the study area which are associated with the presence of low resistivity/unconsolidated rocks. Similarly, the iso-anomaly contour maps of 36 m, 54 m, and 80 m have low resistivity closures in the southern portion of study area which are gradually decreasing from shallow surface to 80 m. The iso-anomaly contour maps of 107 m, 143 m, 170 m, and 205 m

depths have the closure of high electric field values in the northern portion of study area which are associated with the presence of hard rock, i.e., sandstone. Similarly, the closure of low electric field values is found in the middle portion of study area as shown in the 107 m depth map, which is gradually increasing towards the south that can be observed in 143 m, 170 m, and 205 m in the subsurface.

The iso-anomaly contour maps at 250 m, 286 m, 330 m, and 375 m depths have the closure of high electric field values in the northern portion of study area which are associated with the presence of hard rock, i.e., sandstone. Similarly, the patch of low electric field values is found in the middle portion of study area as shown in all figures which is gradually increasing towards the south. Similarly, in the iso-anomaly contour maps of audio-magnetotelluric data from 420 m to the depth of 500 m, the patch of low electric field values gradually increases from 420 m depth to 482 m. Then, this path shifts to the extreme southern portion of the study area which shows the presence of hard rocks in the central part of study area at a depth of 500 m. Comparable results were revealed by the 1D Vertical Electrical Sounding observations.

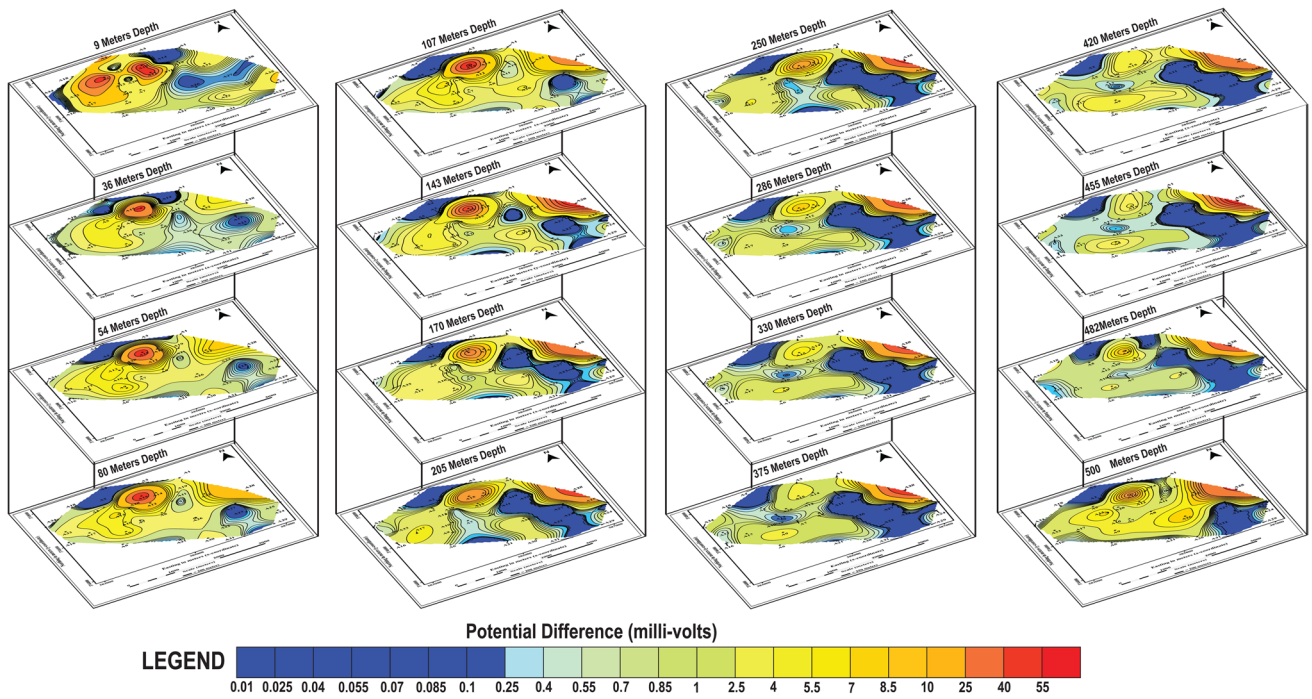


Fig. 8 Overlay of 1D AMT maps at 9 m, 36 m, 54 m, 80 m, 107 m, 143 m, 170 m, 205 m, 250 m, 286 m, 330 m, 375 m, 420 m, 455 m, 480 m, and 500 m

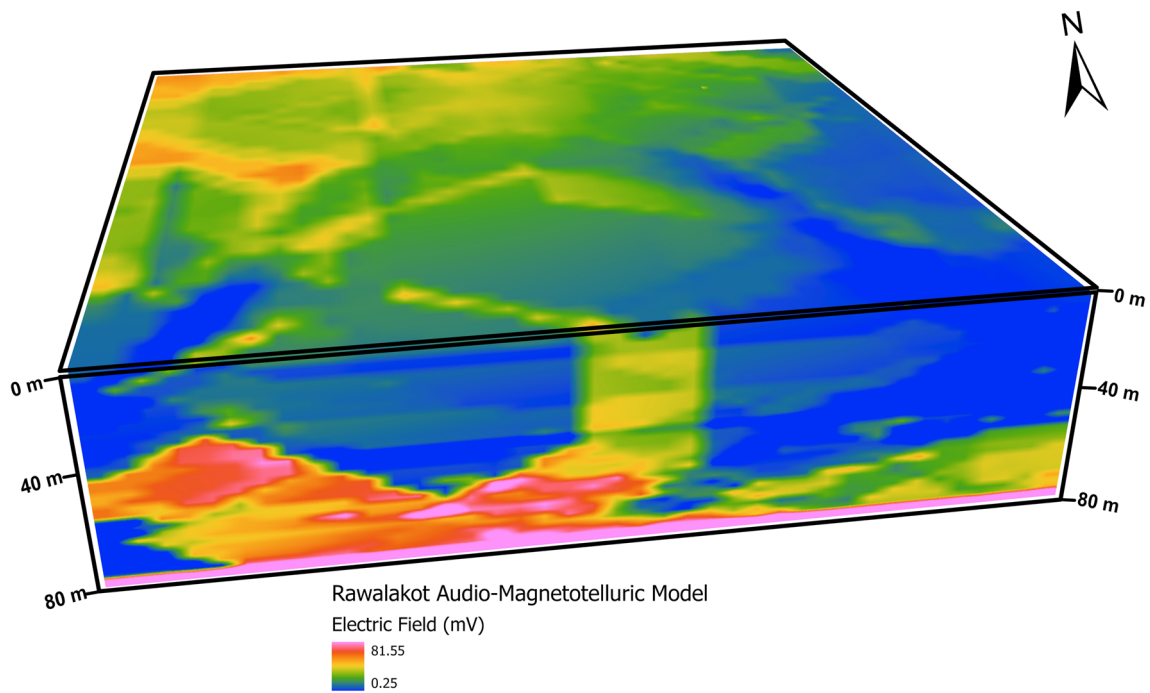


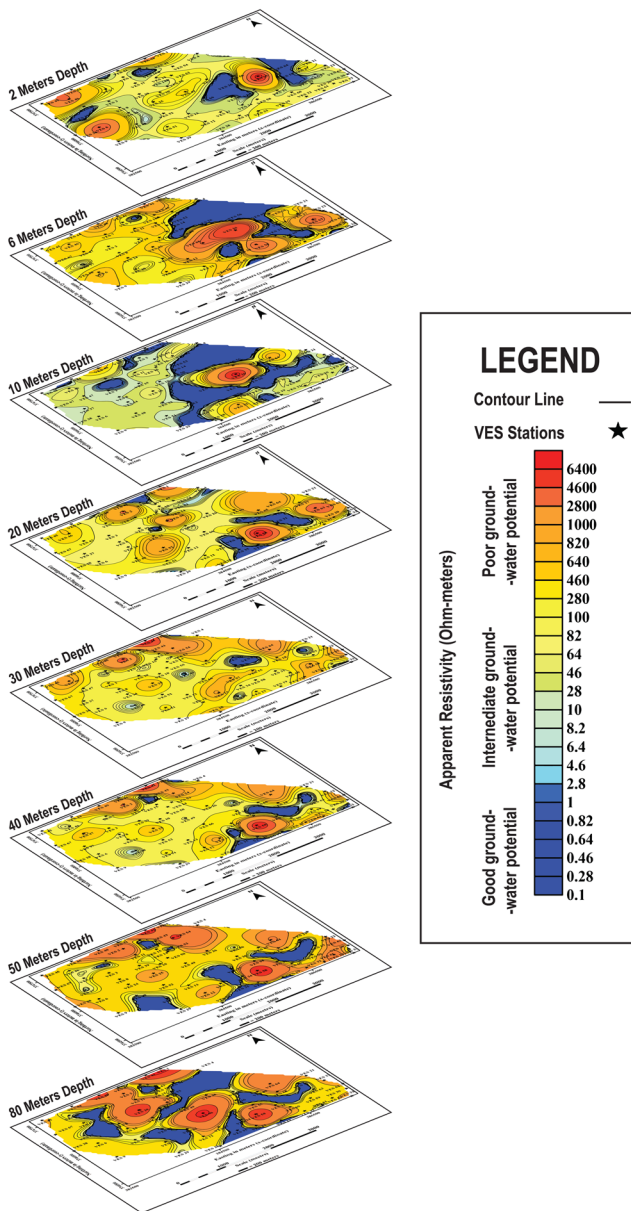
Fig. 9 3D inversion model of audio-magnetotelluric data of the study area

3D audio-magnetotelluric survey model

The three-dimensional model of audio-magnetotelluric survey of study area was prepared using Arc GIS Pro software. The total depth achieved in the survey was 80 m. Total number of 34 AMT stations were established in the study area. The excel database was imported in the Arc GIS Pro. The “Empirical Bayesian Kriging 3D” tool of “geoprocessing” was used to prepare the 2D contour maps at different depths.

Then, “GD Layer 3D to NetCDF” tool was used to prepare the 3D model of the study area up to the depth of 500 m in subsurface. Figure 9 represents the 3D model of AMT data of study area. This model validates the findings of ERS model and shows the distribution of intermediate-to-hard rocks on the northern part of study area due to the presence of sandstone, mudstone, and siltstone of Murree Formation. Whereas, the southern part of study area shows the

ELECTRICAL RESISTIVITY SURVEY



AUDIO-MAGNETOTELLURIC SURVEY

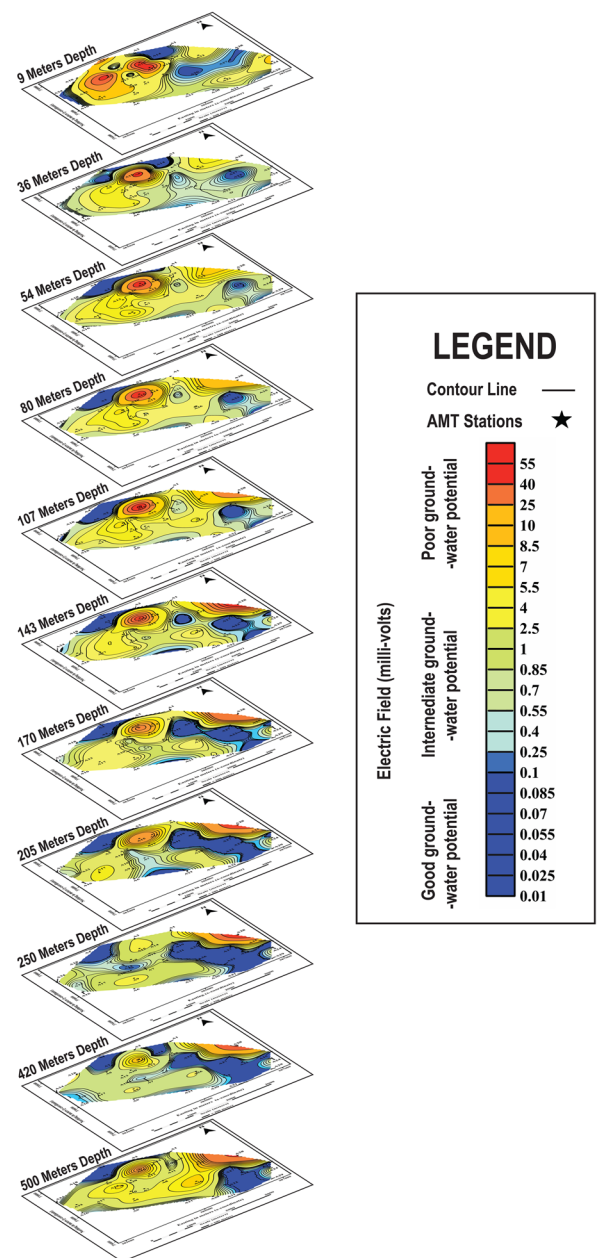


Fig. 10 Comparison of ERS and AMT results

Table 3 Physiochemical parameters of water samples from study area

WHO Standards	NGVS 6.5 to 8.5	NGVS 125–350	<75	<500	<1000	NGVS	Cl	Mg	SO ₄	NO ₃	Na	K	Alkalinity	NGVS -ve	Total coliform	Water Type	Salinity Hazard	Result			
Station Name	E.C	pH	Turbidity	HCO ₃	Ca	Hardness	TDS	CO ₃	CO ₃	Cl	Mg	SO ₄	NO ₃	Na	K	Alkalinity	NGVS -ve	Total coliform	Water Type	Salinity Hazard	Result
Sample 1	384,984.99 3,747,857.63	7.92	1.9	290	80	300	400	BDL	BDL	10	24	39	0.1	30	0.5	290	Negative	Ca-HCO ₃	Medium	Safe	
Sample 2	384,457.73 3,746,493.27	7.94	2.2	260	76	270	396	BDL	BDL	27	19	37	0.4	32	0.3	260	Negative	Ca-HCO ₃	Medium	Safe	
Sample 3	384,579.43 3,745,999.39	7.86	1.4	320	104	340	446	BDL	BDL	24	19	0.5	0.3	10	0.6	320	Positive	Ca-HCO ₃	High	Unsafe	
Sample 4	385,131.16 3,746,247.79	7.4	2.7	220	64	230	315	BDL	BDL	24	17	20	0.3	21	0	220	Negative	Ca-HCO ₃	Medium	Safe	
Sample 5	385,396.94 3,746,189.13	7.48	0.5	330	100	350	456	BDL	BDL	27	24	0.6	0.1	12	0.1	330	Negative	Ca-HCO ₃	High	Safe	
Sample 6	385,364.10 3,747,149.93	7.98	0.5	340	124	360	662	BDL	BDL	48	12	0.6	0.2	25	0.5	340	Negative	Ca-HCO ₃	High	Safe	
Sample 7	385,857.33 3,745,845.35	7.9	1.2	350	128	360	575	BDL	BDL	29	10	15	0.2	21	0.6	350	Positive	Ca-HCO ₃	High	Unsafe	
Sample 8	385,162.10 3,746,971.60	7.86	0.85	290	84	310	499	BDL	BDL	68	24	0.5	0.1	37	1.9	290	Negative	Ca-HCO ₃	High	Safe	
Sample 9	384,981.81 3,746,753.09	7.25	2.9	280	68	290	394	BDL	BDL	24	29	46	0.4	33	1.6	280	Negative	Ca-HCO ₃	Medium	Safe	
Sample 10	385,243.58 3,747,589.45	7.44	0.8	270	80	280	338	BDL	BDL	22	19.44	0.6	0.6	14	0.5	270	Negative	Ca-HCO ₃	Medium	Safe	
Sample 11	385,693.04 3,745,341.61	7.6	0.55	280	100	300	410	BDL	BDL	24	12.15	9	0.3	11	0.6	280	Positive	Ca-HCO ₃	Medium	Unsafe	
Sample 12	385,949.38 3,744,646.52	7.42	1.2	290	112	310	443	BDL	BDL	27	7.29	7	0.3	12	1.2	290	Negative	Ca-HCO ₃	High	Safe	
Sample 13	386,124.92 3,744,622.23	7.47	0.2	330	116	350	459.25	BDL	BDL	31	14.58	6	0.2	15	0.5	330	Negative	Ca-HCO ₃	High	Safe	
Sample 14	386,922.22 3,744,349.90	7.78	0.45	350	120	360	471.35	BDL	BDL	24	14.58	5	0.6	15	0.7	350	Positive	Ca-HCO ₃	High	Unsafe	
Sample 15	384,900.99 3,746,802.86	7.51	0.85	290	84	300	416	BDL	BDL	24	21.87	29	0.6	27	0.9	290	Negative	Ca-HCO ₃	High	Safe	
Sample 16	386,651.81 3,744,024.85	7.56	2.3	390	140	420	652	BDL	BDL	22	17	37	0.4	19	0.1	390	Positive	Ca-HCO ₃	High	Unsafe	
Sample 17	386,272.34 3,744,567.24	7.64	4.0	280	84	290	523	BDL	BDL	43	19.44	12	0.2	30	0.2	280	Positive	Ca-HCO ₃	High	Unsafe	
Sample 18	387,300.48 3,744,484.04	7.12	0.8	270	80	280	393	BDL	BDL	17	19.44	14	0.1	14	0.4	270	Positive	Ca-HCO ₃	Medium	Unsafe	

Table 3 (continued)

WHO Standards	NGVS 6.5 to 8.5	<5	125–350	<75	<500	<1000	NGVS	<250	<50	<250	<50	<200	12	NGVS	-ve	Ca-HCO ₃	Medium	Safe
Sample 19	387,574.83 3,744,675.98	656	250	76	260	360	BDL	21	17	60	0.9	39	0.4	250	Negative	Ca-HCO ₃	Medium	Safe
Sample 20	387,246.08 3,745,204.42	1220	340	80	370	671	BDL	19	17	9	0.2	48	2.1	340	Negative	Ca-HCO ₃	High	Safe
Sample 21	387,038.00 3,745,683.76	844	230	72	240	464.2	BDL	29	14	8	0.3	10	0.6	230	Positive	Ca-HCO ₃	High	Unsafe
Sample 22	386,578.04 3,746,145.04	771	360	100	380	424	BDL	17	31	51	1.2	27	1.1	360	Positive	Ca-HCO ₃	High	Unsafe
Sample 23	385,602.68 3,746,830.99	820	310	68	330	451	BDL	34	38	9	0.3	19	0.7	310	Negative	Ca-HCO ₃	High	Safe
Sample 24	385,926.52 3,747,448.15	616	260	64	270	338.8	BDL	16	26	71	1.6	43	1.6	260	Positive	Ca-HCO ₃	Medium	Unsafe
Sample 25	385,384.49 3,747,382.58	955	340	88	360	525	BDL	26	34	19	1	18	0.9	340	Negative	Ca-HCO ₃	High	Safe
Sample 26	383,566.55 3,746,332.02	826	300	80	320	454	BDL	22	29	21	0.9	17	0.1	300	Negative	Ca-HCO ₃	High	Safe
Sample 27	384,033.55 3,746,384.98	912	280	60	290	501	BDL	27	34	56	0.2	40	0.2	280	Positive	Ca-HCO ₃	High	Unsafe
Sample 28	383,585.74 3,746,334.55	768	290	76	300	422	BDL	19	27	15	0.3	15	0.1	290	Negative	Ca-HCO ₃	High	Safe
Sample 29	383,225.03 3,746,250.14	686	250	56	260	377	BDL	14	29	46	0.8	28	0.1	250	Negative	Ca-HCO ₃	Medium	Safe
Sample 30	382,687.03 3,746,136.43	859	330	104	350	472	BDL	29	22	18	0.6	19	0.1	330	Positive	Ca-HCO ₃	High	Unsafe
Sample 31	382,054.45 3,745,992.76	728	270	80	280	400	BDL	43	19	20	0.4	34	0.9	270	Positive	Ca-HCO ₃	Medium	Unsafe
Sample 32	382,098.12 3,746,432.83	864	350	108	370	475	BDL	21	24	6	0.2	8	0.1	350	Positive	Ca-HCO ₃	High	Unsafe
Sample 33	382,174.68 3,746,898.79	832	340	124	350	457	BDL	24	10	7	0.1	13	1.4	340	Positive	Ca-HCO ₃	High	Unsafe
Sample 34	382,315.02 3,747,772.30	1151	410	120	430	633	BDL	41	32	20	0.6	27	0.6	410	Positive	Ca-HCO ₃	High	Unsafe
Sample 35	382,729.62 3,747,871.64	735	280	88	300	404	BDL	21	19	44	0.5	27	0.1	280	Negative	Ca-HCO ₃	Medium	Safe
Sample 36	382,769.94 3,748,657.78	940	270	76	290	417	BDL	31	24	58	1	41	0.2	270	Negative	Ca-HCO ₃	High	Safe
Sample 37	384,517.71 3,748,369.23	948	280	88	290	521	BDL	24	17	19	0.7	21	0.6	280	Negative	Ca-HCO ₃	High	Safe

Table 3 (continued)

WHO Standards	NGVS 6.5 to 8.5	NGVS <5	125–350	<75	<500	<1000	NGVS <250	<50	<250	<50	<200	12	NGVS -ve	Ca-HCO ₃	High	Safe	
Sample 38	384,155.74	775	7.37	0.7	300	76	320	426.25	BDL	19	32	11	0.8	9	0.1	300	Safe
	3,747,444.49																
Sample 39	384,245.93	689	7.48	1.6	310	60	320	378.95	BDL	26	41	12	0.4	19	0.3	310	Medium
	3,746,568.71																Safe
Minimum		574	7.12	0.2	220	56	230	315		10	7.29	0.5	0.1	8	0	220	
Maximum		1220	7.98	40	410	140	430	671		68	41	71	1.6	48	2.1	410	
Mean		836.02	7.65	4.01	302.05	89.4	317.43	456.94		26.61	22.04	22.02	0.47	23.07	0.60	302.05	
Standard deviation		158.85	0.23	8.39	41.94	21.4	45.64	87.17		10.44	8.03	19.43	0.34	10.66	0.53	41.94	

groundwater potential due to the presence of unconsolidated rocks of surficial deposits like clay, silt, sand, and gravels.

Comparison of 1D electrical resistivity survey and 1D audio-magnetotelluric survey

The comparison of 1D electrical resistivity survey and 1D audio-magnetotelluric survey was made to understand the distribution of subsurface rocks in the study area. The total number of 1D ERS stations was 67, while that of AMT survey was 34. Figure 10 demonstrates the comparison of ERS and AMT surveys. The left portion of diagram shows the apparent resistivity maps at 2, 6, 10, 20, 30, 40, 50, and 80 m depth, while the right portion of diagram show the iso-electric field maps at 9, 36, 54, 80, 107, 143, 176, 205, 250, 420, and 500 m, respectively. The iso-resistivity maps show the distribution of intermediate-to-hard rocks on the northern portion of study area which are associated with sandstone and mudstone of Murree Formation, while low resistivity rocks are distributed in the southern portion of study area which are associated with unconsolidated clay, silt, sand, and gravels of surficial deposits.

Similarly, the iso-electric field audio-magnetotelluric maps from shallow depth to 500 m were prepared to obtain information about subsurface rocks. The audio-magnetotelluric maps show the distribution of intermediate-to-hard rocks on the northern portion of study area which are associated with sandstone and mudstone of Murree Formation. Whereas, the patch of low electric field can be observed in the southern portion of study area which are associated with the unconsolidated rocks like clay, silt, sand, and gravels of surficial deposits. The electrical resistivity survey and audio-magnetotelluric survey cross-validate and match closely to each other.

Physiochemical parameters

A total 39 water samples were analyzed from the Rawalakot city municipality to investigate their chemical and biological properties. Among which, 23 water samples were found to be safe, whereas 16 water samples were classified as unsafe for drinking purpose. All 23 water samples have found “Positive” results of “Total Coliforms”. The total coliforms are normally found in soil, plants, and warm-blooded animals. In case of drinking water, their presence typically points out towards the potential contaminations of pathogens. The water samples with total coliforms should be disinfected instantly for drinking purpose. The sample no. 3, 7, 11, 14, 16, 17, 18, 21, 22, 24, 27, 30, 31, 32, 33, and 34 are marked as unsafe due to the micro-biological contamination. The source-wise distribution of water samples and their physio-chemical results along with their locations are given in Tables 2

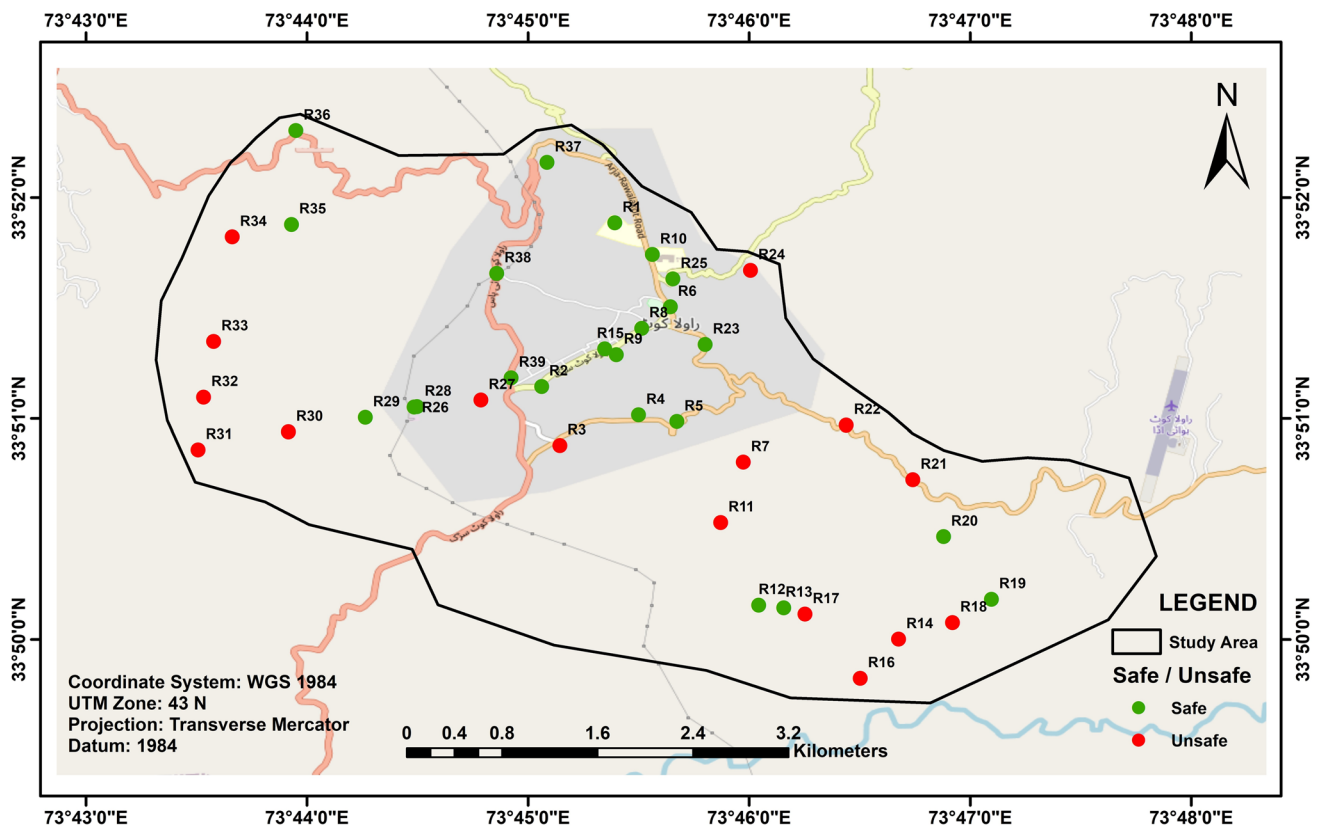


Fig. 11 Groundwater quality map of study area with marked safe and unsafe drinking water samples

and 3, respectively. It is observed that drinking water samples obtained from western and southeastern part of study area are mainly contaminated, whereas the drinking water samples obtained from central and northeastern part of study area are safe for drinking purpose. The groundwater contamination was found in Galiat, Tarar, Chaitri, Kowas, Khrick, Bathnara, and Pothi-Bala areas. The first 38 groundwater samples belong to the Ca–HCO₃ water type, while last groundwater sample belongs to the Mg–HCO₃ water type. Moreover, considering the irrigation scope, 26 groundwater samples were marked with high salinity hazard, while 13 groundwater samples were marked with medium salinity hazard in the study area. The groundwater quality map with the help of dot density map is given in Fig. 11. Table 2 explains the source-wise distribution of water samples from study area.

Conclusion

The integrated approach of two geophysical methods, e.g., 1D electrical resistivity survey and 2D audio-magnetotelluric survey, has revealed the demarcation of groundwater potential from shallow depth up to 180 m at Rawalakot

city municipality, Azad Kashmir. The integration of both techniques has minimized the limitations and ambiguities of geophysical methods. The electrical resistivity survey demarcated the low resistivity material at the central part of study area at depth of 2 m. This patch of low resistivity material extends further up to the depth of 10 m in the subsurface. The low resistivity patch further extends towards the southern portion of study area up to the depth of 50 m. Finally, at the depth of 80 m, the good groundwater potential was demarcated which was associated with the low resistivity material at central portion of study area. Similarly, the audio-magnetotelluric maps were acquired up to the depth of 500 m. The iso-electric field maps of AMT data revealed the presence of low resistivity material at central and southern part of the study area. Both surveys revealed that there is a good groundwater potential at the central and southeastern part of the study area with three-to-five subsurface layers which are boulder clay, clay, clay (very dry), clayey sand, dry sandy soil, gravel (saturated), mudstone, sand and gravel (saturated), sandstone, sandstone (weathered), sandy clay, siltstone, and top soil. The borehole data acquired from study area match closely with the interpreted lithology. The deep groundwater potential zones were demarcated from 50 m in the subsurface to

480 m as interpreted by AMT data in the southern part of study area. Different fractures were also delineated in the study area with depth ranging from 50 m to 300 m in the subsurface. Similarly, the 1D iso-anomaly contour maps of ERS data were compared with the 1D iso-anomaly contour maps of AMT data. Their comparison leads to the accuracy and validation of both surveys. In this way, the 1D and 2D data demarcated the presence of subsurface groundwater potential at the central and southeastern portion of the study area. The water samples acquired from the study area revealed that among 39 water samples 16 water samples were found to be unsafe for drinking purpose due to the total coliforms' contamination. While, 23 water samples were found to be safe for drinking purpose.

Supplementary Information The online version contains supplementary material available at <https://doi.org/10.1007/s12665-023-11368-2>.

Acknowledgements The authors thank the Higher Education Commission (HEC), Pakistan for providing the financial support under NRPJ Project No. 17374 and the Director, Institute of Geology, University of Azad Jammu and Kashmir, Muzaffarabad, for giving the transport and laboratory facilities. The authors sincerely thank the anonymous reviewers for their insightful suggestions that improved the manuscript and the editors for constructive comments.

Author contributions All the authors contributed to the current study conception and design. AYK: conceptualization, formal analysis, field planning, methodology, and writing original draft. Dr. AN: resources, project administration, supervision, validation, and reviewing. Dr. UBN: review and editing.

Funding This work was supported by Higher Education Commission, Pakistan under National Research Program for Universities Grant Number 20–17374/NRPJ/R&D/HEC/2021. The authors acknowledge the financial support, which helped in planning, implementation, and current study.

Data availability The data is available with first author.

Declarations

Conflict of interest The authors declare that they have no conflict of interests.

References

- Adeniji AA, Ajani OO, Adagunodo TA, Agbolade JO, Ayeni AM (2023) Application of Dar-Zarrouk parameters for groundwater protective potential within the crystalline basement formation, Southwestern Nigeria. *J Sci Islamic Republic of Iran* 33(3):245–257
- Agyemang VO (2020) Application of magnetotelluric geophysical technique in delineation of zones of high groundwater potential for borehole drilling in five communities in the Agona East District. *Ghana Appl Water Sci* 10(6):1–6
- Agyemang VO (2022) Groundwater exploration by magnetotelluric method within the birimian rocks of mankessim. *Ghana Appl Water Sci* 12(3):26
- Aizawa K, Ogawa Y, Ishido T (2009) Groundwater flow and hydrothermal systems within volcanic edifices: delineation by electric self-potential and magnetotellurics. *J Geophys Res* 114(B1)
- Ako B (1983) Osundu V (1986) Electrical resistivity survey of the Kerri-Kerri formation, Darazo, Nigeria. *J African Earth Sci* 5(5):527–534
- Arshad M, Cheema J, Ahmed S (2007) Determination of lithology and groundwater quality using electrical resistivity survey. *Int J Agric Biol* 9(1):143–146
- Arulprakasam V, Sivakumar R, Gowtham B (2013) Determination of hydraulic characteristics using electrical resistivity methods—a case study from Vanur watershed, Villupuram district. *Tamil Nadu J Appl Geol Geophys* 1:10–14
- Azeem MW, Rehman K, Rehman NU, Farooq U, Arshad A (2021) Delineation of sinkhole in evaporite deposits using electrical resistivity survey: a case study of southern Kohat Plateau. *Pakistan Arab J Geosci* 14(4):307
- Bobachev A, Modin I, Shevnev V (2003) IPI2Win software version 3.0. 1a. Geoscan-M Ltd., Moscow State University, Geological Faculty, Department of Geophysics. Moscow, Russia.
- Bremmer SE, Tobin HJ (2016) Detailed Three Dimensional Structural Analysis of the Outer Nankai Accretionary Wedge, Kii-Kumano Region, Southwest Japan. In *AGU Fall Meeting Abstracts* (Vol. 2016, pp. T31C-2902).
- Calkins JA, TW O, SKM A (1975) geology of the southern Himalaya in Hazara, Pakistan and Adjacent areas.
- Chaudhry M, Spencer D, Ghazanfar M, Hussain S, Dawood H (1997) The location of the main central thrust in the Northwest Himalaya of Pakistan: tectonic implications. *Geol Bull Punjab Univ* 31:1–19
- Chouteau M, Krivochieva S, Castillo RR, Moran TG, Jouanne V (1994) Study of the Santa Catarina aquifer system (Mexico Basin) using magnetotelluric soundings. *J Appl Geophys* 31(1–4):85–106
- Chukwuma E, Orakwe L, Anizoba D, Amaefule D, Odoh C, Nzediegwu C (2015) Geo-electric groundwater vulnerability assessment of overburdened aquifers at Awka in Anambra State, south-eastern Nigeria. *Euro J Biotechnol Biosci* 3(1):29–34
- Franks F (2000) *Water: a matrix of life* (Vol. 21): Royal Society of Chemistry
- Gautam VK, Pande CB, Kothari M, Singh PK, Agrawal A (2023) Exploration of groundwater potential zones mapping for hard rock region in the Jakhm river basin using geospatial techniques and aquifer parameters. *Adv Space Res* 71(6):2892–2908
- Gavillot Y, Meigs A, Yule D, Heermance R, Rittenour T, Madugo C, Malik M (2016) Shortening rate and Holocene surface rupture on the Riasi fault system in the Kashmir Himalaya: active thrusting within the Northwest Himalayan orogenic wedge. *Bulletin*, 128(7–8), 1070–1094
- Gelsey K, Chang H, Ramirez D (2023) Effects of landscape characteristics, anthropogenic factors, and seasonality on water quality in Portland. *Oregon Environ Monitoring and Assessment* 195(1):219
- Gernez S, Bouchedda A, Gloaguen E, Paradis D (2019) Comparison between hydraulic conductivity anisotropy and electrical resistivity anisotropy from tomography inverse modeling. *Front Environ Sci* 7:67
- Hameed F, Khan MR, Dentith M (2023) Crustal study based on integrated geophysical techniques in the Northwestern Himalayas, Pakistan. *Geological Journal*
- Hamzah U, Yaacup R, Samsudin AR, Ayub MS (2006) Electrical imaging of the groundwater aquifer at Banting, Selangor, Malaysia. *Environ Geol* 49:1156–1162
- Hasan M, Shang Y, Akhter G, Jin W (2019) Application of VES and ERT for delineation of fresh-saline interface in alluvial aquifers of Lower Bari Doab, Pakistan. *J Appl Geophys* 164:200–213

- Hasan M, Shang Y (2023) Investigating the groundwater resources of weathered bedrock using an integrated geophysical approach. *Environ Earth Sci* 82(9):213
- Hayder R, Hafeez M, Ahmad P, Memon N, Khandaker MU, Elqahtani ZM, . . . Ahmed MN (2023) Heavy Metal Estimation and Quality Assurance Parameters for Water Resources in the Northern Region of Pakistan. *Water*, 15(1), 77
- Henriet JP (1976) Direct applications of the Dar Zarrouk param in ground water surveys. *Geophys Prospect* 24(2):344–353
- Hernance JF, Thayer RE (1975) The telluric-magnetotelluric method. *Geophysics* 40(4):664–668
- Hespanhol I, Prost A (1994) WHO guidelines and national standards for reuse and water quality. *Water Res* 28(1):119–124
- Hidayatika A, Mulyasari R, Yogi IS, Prabowo AP, Rasimeng S (2022) The initiation study on the gold potential resources at West Coast Area in Lampung Province, Indonesia. *J Eng Sci Res* 4(1):40–44
- Huang J, Ma C, Sun Y (2021) 2D Magnetotelluric forward modeling for deep buried water-rich fault and its application. *J Appl Geophys* 192:104403
- Hujakulova D, Ulashov SM, Gulomova D (2021) Technology of deodorization of soyabean oil. *Galaxy Int Interdisciplinary Res J* 9(12):171–174
- Hussain A, Saeed G, Akhtar SS (2014) Geological Map of the Rawalakot Area, Bagh and Rawalakot Districts, AJK. Geological Survey of Pakistan, Preliminary Map Series (Azad Jammu & Kashmir) Geological Map Series, Vol. VI (20)
- Javaid Z, Ibrahim M, Mahmood A, Bajwa AA (2023) Pesticide contamination of potable water and its correlation with water quality in different regions of Punjab. *Pakistan Water* 15(3):543
- Kelbert A, Balch CC, Pulkkinen A, Egbert GD, Love JJ, Rigler EJ, Fujii I (2017) Methodology for time-domain estimation of storm time geoelectric fields using the 3-D magnetotelluric response tensors. *Space Weather* 15(7):874–894
- Khan MR, Hameed F, Mughal MS, Basharat M, Mustafa S (2016) Tectonic study of the Sub-Himalayas based on geophysical data in Azad Jammu and Kashmir and northern Pakistan. *J Earth Sci* 27:981–988
- Kirkby A (2019) Developing metadata standards for time series magnetotelluric data. *Preview* 2019(199):49–53
- Kouadio KL, Liu R, Mi B, Liu C-m (2022) pyCSAMT: An alternative Python toolbox for groundwater exploration using controlled source audio-frequency magnetotelluric. *J Appl Geophys* 201:104647
- Latif M (1970) Explanatory notes on the Geology of South Eastern Hazara, to accompany the revised Geological Map. Wien Jb. Geol. BA, Sonderb, 15
- Lee GF, Jones RA, Newbry BW (1982) Water quality standards and water quality. *Journal (Water Pollution Control Federation)*, 1131–1138
- Li J, Pang Z, Kong Y, Lin F, Wang Y, Wang G, Lv L (2017) An integrated magnetotelluric and gamma exploration of groundwater in fractured granite for small-scale freshwater supply: a case study from the Boshan region, Shandong Province, China. *Environ Earth Sci* 76:1–12
- Lisa M, Khwaja A, Shehzad F (2006) Recent seismic activity in Muzaffarabad and its surrounding areas. *Pak J Meteorol* 3:7–11
- Lu D, Huang D, Xu C (2021) Estimation of hydraulic conductivity by using pumping test data and electrical resistivity data in faults zone. *Ecol Ind* 129:107861
- Mahmud S, Hamza S, Irfan M, Huda SN-u, Burke F, Qadir A (2022) Investigation of groundwater resources using electrical resistivity sounding and Dar Zarrouk parameters for Uthal Balochistan, Pakistan. *Groundwater for sustainable development*, 17, 100738
- Makhmudov R, Majidov KK, Usmanova M, Ulashov SM, Niyozov S (2021) Characteristics of catalpa plant as raw material for oil extraction. *Am J Eng Technol* 3(03):70–75
- Mekkawi MM, Abd-El-Nabi SH, Farag KS, Abd Elhamid MY (2022) Geothermal resources prospecting using magnetotelluric and magnetic methods at Al Ain AlSukhuna-Al Galala Albahariya area, Gulf of Suez. *Egypt J African Earth Sci* 190:104522
- Mohamed A, Othman A, Galal WF, Abdelrady A (2023) Integrated geophysical approach of groundwater potential in Wadi Ranyah, Saudi Arabia, using gravity, electrical resistivity, and remote-sensing techniques. *Remote Sensing*, 15(7), 1808
- Mohammed MA, Szabó NP, Szűcs P (2023) Exploring hydrogeological parameters by integration of geophysical and hydrogeological methods in northern Khartoum state. *Sudan Groundwater Sustain Dev* 20:100891
- Moulds M, Gould I, Wright I, Webster D, Magnone D (2023) Use of electrical resistivity tomography to reveal the shallow freshwater–saline interface in The Fens coastal groundwater, eastern England (UK). *Hydrogeol J* 1–15
- Mualem Y (1986) Hydraulic conductivity of unsaturated soils: Prediction and formulas. *Methods oil Anal* 5, 799–823
- Muchingami I, Hlatywayo D, Nel J, Chuma C (2012) Electrical resistivity survey for groundwater investigations and shallow subsurface evaluation of the basaltic-greenstone formation of the urban Bulawayo aquifer. *Phys Chem Earth Parts a/b/c* 50:44–51
- Nair AM, Prasad KR, Srinivas R (2022) Groundwater vulnerability assessment of an urban coastal phreatic aquifer in India using GIS-based DRASTIC model. *Groundw Sustain Dev* 19:100810
- Niaz A, Bibi T, Qureshi JA, Rahim S, Hameed F, Shedayi AA (2021) A comparison between schlumberger and wenner configurations in delineating subsurface water bearing zones: a case study of Rawalakot Azad Jammu and Kashmir, Pakistan. *Int J Econ Environ Geol* 12(3):25–31
- Niaz A, Khan M, Asghar A, Mustafa S, Hameed F (2013) Determination of groundwater potential in Mirpur Azad Jammu and Kashmir, Pakistan using geoelectric method vertical electrical sounding. *Int J Sci Eng Res* 4:2229–5518
- Niaz A, Khan M, Mustafa S, Hameed F (2016). Determination of aquifer properties and vulnerability mapping by using geoelectrical investigation of parts of Sub-Himalayas, Bhimber, Azad Jammu and Kashmir, Pakistan
- Niaz A, Khan MR, Ijaz U, Yasin M, Hameed F (2018) Determination of groundwater potential by using geoelectrical method and petrographic analysis in Rawalakot and adjacent areas of Azad Kashmir, sub-Himalayas, Pakistan. *Arab J Geosci* 11:1–13
- Niaz A, Khan MR, Nisar UB, Khan S, Mustafa S, Hameed F, . . . Rizwan M (2017) The study of aquifers potential and contamination based on geoelectric technique and chemical analysis in Mirpur Azad Jammu and Kashmir, Pakistan. *J Himalayan Earth Sci*, 50(2), 60–73
- Nisar UB, Khan MR, Khan S, Farooq M, Mughal MR, Ahmed KA, . . . Niaz A (2018) Quaternary Paleo-depositional Environments in relation to Ground water occurrence in lesser Himalayan Region, Pakistan. *J Himalayan Earth Sci* 51(1)
- Nisar UB, Khan MJ, Imran M, Khan MR, Farooq M, Ehsan SA., . . . & Manzoor T (2021) Groundwater investigations in the Hattar industrial estate and its vicinity, Haripur district, Pakistan: An integrated approach. *Kuwait J Sci* 48(1).
- Nisar UB, Farooq M, Khan S, Pant RR, Satti IA, Wahid A, . . . & Butt FM (2023) Integrated Geophysical and Geotechnical Approaches for Evaluating Dam Seepage in Lesser Himalayan Region of Pakistan. *Geofluids*, 2023.
- Nowroozi AA, Horrocks SB, Henderson P (1999) Saltwater intrusion into the freshwater aquifer in the eastern shore of Virginia: a reconnaissance electrical resistivity survey. *J Appl Geophys* 42(1):1–22

- Nwachukwu S, Bello R, Balogun AO (2019) Evaluation of groundwater potentials of Orogun, South-South part of Nigeria using electrical resistivity method. *Appl Water Sci* 9(8):184
- Nyambar INa, Mohan Viswanathan P (2023) Assessment on urban lakes along the coastal region of Miri, NW Borneo: implication for hydrochemistry, water quality, and pollution risk. *Environ Sci Pollut Res*, 1–23
- Obiora DN, Ajala AE, Ibuot JC (2015) Evaluation of aquifer protective capacity of overburden unit and soil corrosivity in Makurdi, Benue state, Nigeria, using electrical resistivity method. *J Earth Syst Sci* 124:125–135
- Rahman MM, Haque T, Mahmud A, Al Amin M, Hossain MS, Hasan MY, . . . Bai L (2023) Drinking water quality assessment based on index values incorporating WHO guidelines and Bangladesh standards. *Phys Chem Earth, Parts A/B/C*, 129, 103353
- Riwayat AI, Nazri MAA, Abidin MHZ (2018) Application of electrical resistivity method (ERM) in groundwater exploration. Paper presented at the Journal of Physics: Conference Series
- RockWare I (Producer). (2023). ROCKWORKS. Rockware. <https://www.rockware.com/product/rockworks/>
- Rosas-Carbajal M, Linde N, Peacock J, Zyserman FI, Kalscheuer T, Thiel S (2015) Probabilistic 3-D time-lapse inversion of magnetotelluric data: application to an enhanced geothermal system. *Geophys Suppl Mon Notices R Astronomical Soc* 203(3):1946–1960
- Sajadi P, Singh A, Mukherjee S, Chapi K (2013) Preliminary Results from Subsurface Hydrological Investigations of Dehgolan Plain, Kurdistan, Iran using Geophysical Techniques. Paper presented at the 2012 International SWAT Conference Proceedings
- Searle M, Kahn M (1996) Geological Map of North Pakistan and Adjacent Areas of Northern Ladakh and Western Tibet. (Western Himalaya, Salt Ranges, Kohistan, Karakoram, Hindu Kush), 1: 650 000
- Shah S (2009) Geological Survey of Pakistan. *Stratigraphy Pakistan* 22:245–273
- Simpson F, Bahr K (2021) Nowcasting and validating Earth's electric field response to extreme space weather events using magnetotelluric data: Application to the September 2017 geomagnetic storm and comparison to observed and modeled fields in Scotland. *Space Weather*, 19(1): e2019SW002432
- Singh S, Gautam PK, Kumar P, Biswas A, Sarkar T (2021) Delineating the characteristics of saline water intrusion in the coastal aquifers of Tamil Nadu, India by analysing the Dar-Zarrouk parameters. *Contributions Geophys Geodesy* 51(2):141–163
- Singh U, Sharma PK (2023) Non-invasive Subsurface Groundwater Exploration Techniques. In *Environmental Processes and Management: Tools and Practices for Groundwater* (pp. 1–16): Springer
- Slater L (2007) Near surface electrical characterization of hydraulic conductivity: From petrophysical properties to aquifer geometries—a review. *Surv Geophys* 28:169–197
- Suleman K, Aanuoluwa A, Ogunmola O, Adeoye T, Sunmonu L, Alagbe G, . . . Babarimisa I (2023) Investigation of subsurface contaminants leachate within Ansaru-Islam Secondary School, Ilorin, Nigeria. *IOP Conference Series: Earth and Environmental Science*, 1197, 012011 <https://doi.org/10.1088/1755-1315/1197/1/012011>
- Torrese P, Rainone ML, Colantonio F, Signanini P (2013). Identification and investigation of shallow paleochannels in the Chamelecon Valley (Honduras): 1D vs 2D electrical resistivity surveys. Paper presented at the Symposium on the Application of Geophysics to Engineering and Environmental Problems 2013
- Troisi S, Fallico C, Straface S, Migliari E (2000) Application of kriging with external drift to estimate hydraulic conductivity from electrical-resistivity data in unconsolidated deposits near Montalto Uffugo, Italy. *Hydrogeol J* 8:356–367
- Utom AU, Odoh BI, Okoro AU (2012) Estimation of aquifer transmissivity using Dar Zarrouk parameters derived from surface resistivity measurements: a case history from parts of Enugu Town (Nigeria). *J Water Resour Prot* 4(12):993
- Uwiringiyimana J (2019) Hydrogeophysics for designing the hydrogeophysical conceptual model of a sub-catchment in Maqu. University of Twente, Tibet-China
- Wadia D (1931) The syntaxis of the northwest Himalaya: its rocks, tectonics and orogeny. *Rec Geol Surv India* 65(2):189–220
- Xu Z, Li G, Xin H, Tang J, Lv F (2020) Hydrogeological prospecting in the Da Qaidam area of the Qaidam Basin using the audio-frequency magnetotelluric method. *J Appl Geophys* 182:104179
- Yeh TCJ, Zhu J, Englert A, Guzman A, Flaherty S (2006) A successive linear estimator for electrical resistivity tomography. In: Vereecken, H., Binley, A., Cassiani, G., Revil, A., Titov, K. (eds) *Applied Hydrogeophysics*. NATO Science Series, vol 71. Springer, Dordrecht. https://doi.org/10.1007/978-1-4020-4912-5_3

Publisher's Note Springer Nature remains neutral with regard to jurisdictional claims in published maps and institutional affiliations.

Springer Nature or its licensor (e.g. a society or other partner) holds exclusive rights to this article under a publishing agreement with the author(s) or other rightsholder(s); author self-archiving of the accepted manuscript version of this article is solely governed by the terms of such publishing agreement and applicable law.